CERAMICS

# A general method to synthesize and sinter bulk ceramics in seconds

Chengwei Wang[1]*, Weiwei Ping[1]*, Qiang Bai[1]*, Huachen Cui[2,3]*, Ryan Hensleigh[2,3]*, Ruiliu Wang[1], Alexandra H. Brozena[1], Zhenpeng Xu[2,3], Jiaqi Dai[1], Yong Pei[4], Chaolun Zheng[4], Glenn Pastel[1], Jinlong Gao[1], Xizheng Wang[1], Howard Wang[1], Ji-Cheng Zhao[1], Bao Yang[4], Xiaoyu (Rayne) Zheng[2,3]†, Jian Luo[5]†, Yifei Mo[1]†, Bruce Dunn[6], Liangbing Hu[1,7]†

Ceramics are an important class of materials with widespread applications because of their high thermal, mechanical, and chemical stability. Computational predictions based on first principles methods can be a valuable tool in accelerating materials discovery to develop improved ceramics. It is essential to experimentally confirm the material properties of such predictions. However, materials screening rates are limited by the long processing times and the poor compositional control from volatile element loss in conventional ceramic sintering techniques. To overcome these limitations, we developed an ultrafast high-temperature sintering (UHS) process for the fabrication of ceramic materials by radiative heating under an inert atmosphere. We provide several examples of the UHS process to demonstrate its potential utility and applications, including advancements in solid-state electrolytes, multicomponent structures, and high-throughput materials screening.

Ceramics are widely used in electronics, energy storage, and extreme environments because of their high thermal, mechanical, and chemical stability. The sintering of ceramics is a technology that can be traced back to more than 26,000 years ago (*1*). Conventional ceramic sintering often requires hours of processing time (*2*), which can become an obstacle for the high-throughput discovery of advanced ceramic materials. The long sintering time is particularly problematic in the development of ceramic-based solid-state electrolytes (SSEs)—which are critical for new batteries with improved energy efficiency and safety (*3*, *4*)—because of the severe volatility of Li and Na during sintering (*5*–*9*).

Substantial effort has been devoted to the development of innovative sintering technologies, such as microwave-assisted sintering, spark plasma sintering (SPS), and flash sintering. Microwave-assisted sintering of ceramics often depends on the microwave absorption properties of the materials or uses susceptors (*10*, *11*). The SPS technique requires that dies are used to compress the ceramic while sintering (*12*), which makes it more difficult to sinter specimens with complex three-dimensional (3D) structures. Furthermore, SPS normally produces only one specimen at a time, though special tooling can and has been made to fabricate multiple samples. The more-recently developed flash sintering (*13*), photonic sintering (*14*), and rapid thermal annealing (RTA) (*15*) methods display a high heating rate of ~$10^3$ to $10^4$°C/min. However, flash sintering typically requires expensive Pt electrodes and is material specific. Although flash sintering can be applied to many ceramics, flash sintering conditions depend strongly on the electrical characteristics of the material (*16*), which limits the general applicability of this method as well as its utility for high-throughput processing when a material's properties are unknown. Photonic sintering temperatures are normally too low to sinter ceramics (*14*, *17*). RTA has been used successfully to sinter ZnO (*15*), but this method can only provide a sintering temperature of up to ~1200°C with expensive commercial equipment.

To meet the needs of modern ceramics and foster material innovation, we report a ceramic synthesis method, called ultrafast high-temperature sintering (UHS), that features a uniform temperature distribution, high heating (~$10^3$ to $10^4$°C/min) and cooling rates (up to $10^4$°C/min), and high sintering temperatures (up to 3000°C). The ultrahigh heating rates and temperatures enable ultrafast sintering times of ~10 s (Fig. 1A), far outpacing those of most conventional furnaces. To conduct the process, we directly sandwich a pressed green pellet (Fig. 1B) of ceramic precursor powders between two Joule-heating carbon strips that rapidly heat the pellet through radiation and conduction to form a uniform high-temperature environment (fig. S1) for quick synthesis (solid-state reaction) and reactive sintering (Fig. 1C). In an inert atmosphere, these carbon heating elements can provide a temperature of up to ~3000°C (fig. S2), which is sufficient to synthesize and sinter virtually any ceramic material. The short sintering time also helps to prevent volatile evaporation and undesirable interdiffusion at the interfaces of multilayer structures. Additionally, the technique is scalable because the processing is decoupled from the intrinsic properties of materials (unlike flash sintering; table S3), thereby allowing general and rapid ceramic synthesis and sintering. The UHS process is also compatible with the 3D printing of ceramic precursors, producing novel post-sintering structures in addition to well-defined interfaces between multilayer ceramic compounds. Furthermore, the speed of UHS enables the rapid experimental validation of new material predictions from computation, which facilitates materials discovery spanning a wide range of compositions. Several applications may benefit from this methodology, including thin-film SSEs and battery applications.

In a typical UHS process, the heating elements ramp up from room temperature to the sintering temperature in ~30 s or less (Fig. 2A, bottom), a process that would typically take a conventional furnace several hours to complete (fig. S3). This temperature ramping stage is followed by ~10 s of isothermal sintering and then rapid cooling (in ~5 s). These times and conditions are attractive compared with those of other sintering methods (fig. S4 and table S3) (*11*, *12*, *16*). As a demonstration of the process, we synthesized Ta-doped $Li_{6.5}La_3Zr_{1.5}Ta_{0.5}O_{12}$ (LLZTO), a garnet-type Li-ion–conductive ceramic proposed for SSE applications (*18*). In the UHS technique, the precursors of LLZTO quickly react and densify (Fig. 2A, top) in ~40 s (~30 s of temperature ramping and ~10 s of isothermal sintering), as the temperature of the heater approaches ~1500°C (movie S1). The high sintering temperature and short sintering time of the UHS technique produce a relatively small grain size of 8.5 ± 2.0 μm (Fig. 2B) and a high relative density of ~97% (fig. S5). By contrast, the conventional furnace–sintered garnet features a microstructure with larger grains of 13.5 ± 5 μm (Fig. 2C). This rapid sintering and densification observed in the materials produced by the UHS method may originate from (i) fast kinetics from the high sample temperature, (ii) additional chemical driving force beyond the normal capillary driving force for densification caused by the simultaneous reaction and sintering process, or (iii) the ultrahigh heating rates enhancing the densification rates (*15*, *19*).

In general, sintering involves competition between the coarsening and densification of particles. Surface diffusion can dominate at low temperatures and causes coarsening and neck growth without densification, whereas

[1]Department of Materials Science and Engineering, University of Maryland, College Park, MD 20742, USA. [2]Department of Mechanical Engineering, Virginia Tech, Blacksburg, VA 24061, USA. [3]Departments of Civil and Environmental Engineering and Mechanical and Aerospace Engineering, University of California, Los Angeles, CA 90095, USA. [4]Department of Mechanical Engineering, University of Maryland, College Park, MD 20742, USA. [5]Department of NanoEngineering, Program of Materials Science and Engineering, University of California San Diego, La Jolla, CA 92093, USA. [6]Department of Materials Science and Engineering, University of California, Los Angeles, CA 90095, USA. [7]Center for Materials Innovation, University of Maryland, College Park, MD 20742, USA.
*These authors contributed equally to this work.
†Corresponding author. Email: binghu@umd.edu (L.H.); yfmo@umd.edu (Y.M.); raynexzheng@vt.edu (X.Z.); jluo@ucsd.edu (J.L.)

grain boundary and bulk diffusion are more important at high temperatures, leading to fast densification. The ultrahigh heating rates of UHS bypass the low-temperature region, thereby reducing the coarsening of particles and maintaining a higher capillary driving force for sintering, similar to that observed in other ultrafast heating schemes, such as flash sintering and other exotic heating methods (*15*, *19*). The lower activation energies (fig. S5) also suggest that sintering and grain growth mechanisms in the UHS process are somewhat different from those in conventional sintering methods (*20*). In some cases, particularly for some solid electrolytes of complex chemistries, a small fraction of a liquid can form at the high processing temperature in UHS, which further promotes densification as ultrafast liquid-phase sintering (*21*).

The long sintering time of conventional syntheses can lead to Li loss in garnet SSEs

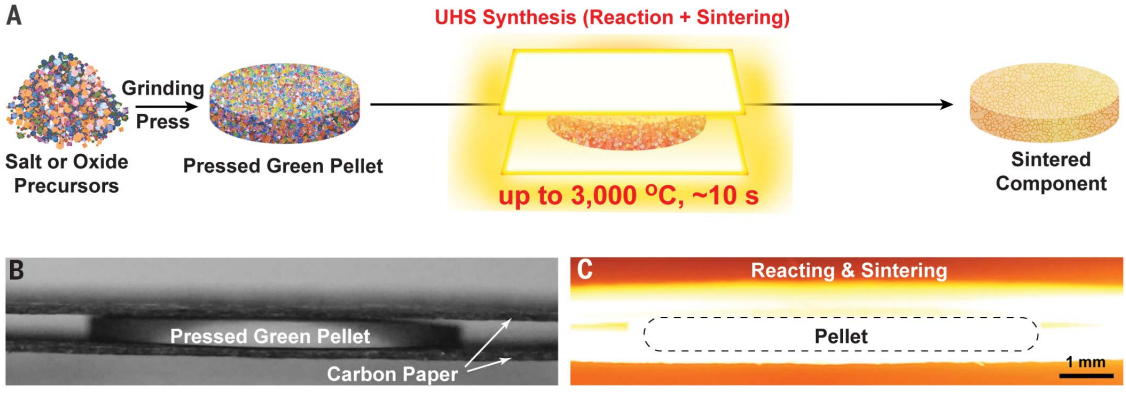


**Fig. 1. Rapid sintering process and setup for ceramic synthesis.** (**A**) Schematic of the UHS synthesis process, in which the pressed green pellet of precursors is directly sintered into a dense ceramic component at a high sintering temperature of up to 3000°C in ~10 s. (**B** and **C**) Photographs of the UHS sintering setup at room temperature without applying current (B), and at ~1500°C (C), in which the closely packed heating strips surrounding the pressed green pellet provide a uniform temperature distribution that enables rapid ceramic sintering.

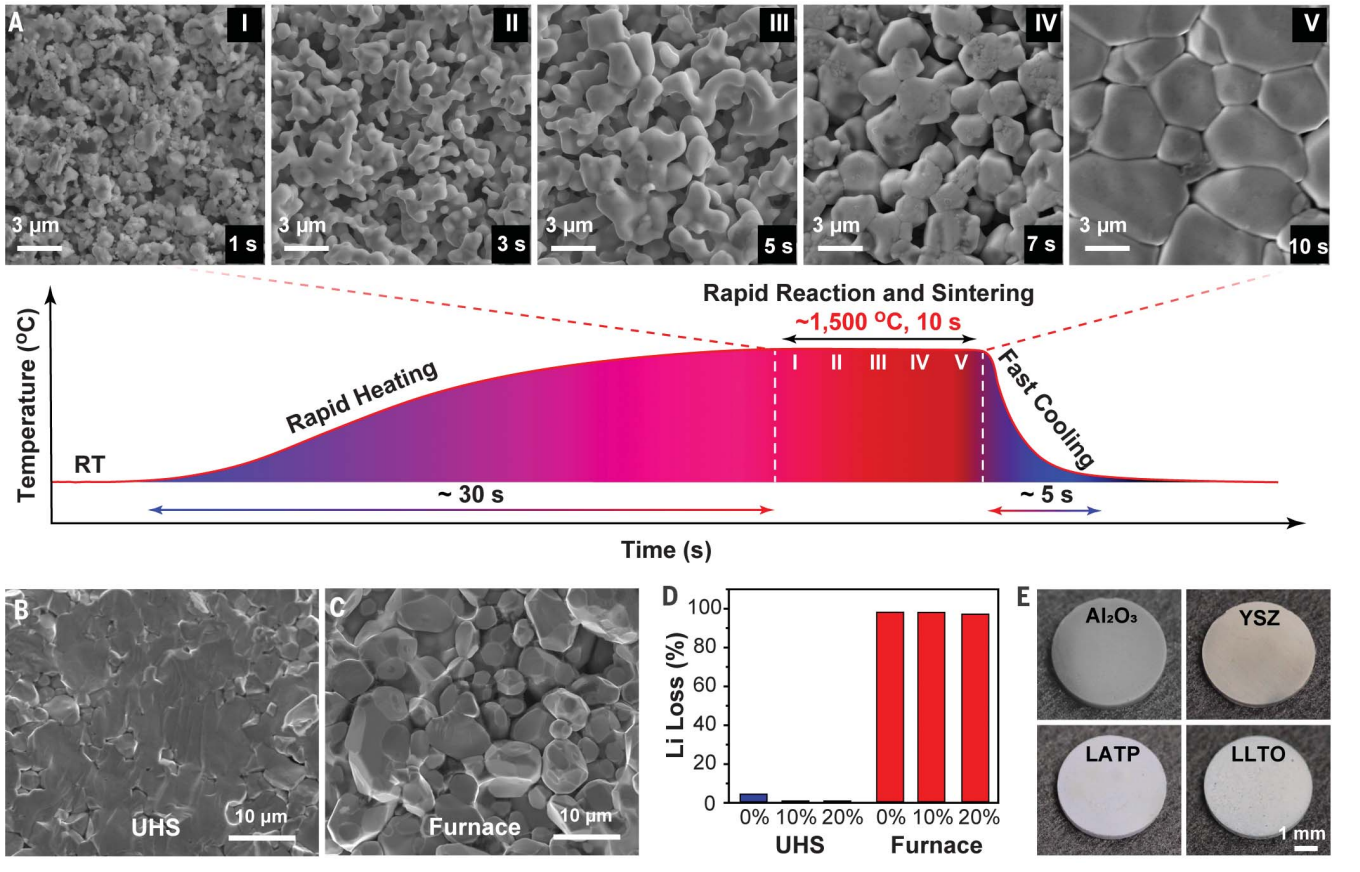


**Fig. 2. Rapid sintering of ceramic materials.** (**A**) Typical temperature profile of the UHS process. The whole process takes <1 min. The SEM images demonstrate the reaction process of the LLZTO ceramic over a 10-s isothermal hold of UHS sintering. RT, room temperature. (**B** and **C**) Fracture cross-sectional SEM images of UHS-sintered (B) and conventional furnace–sintered (C) LLZTO. (**D**) Li loss of different LLZTO samples sintered from precursors with 0, 10, and 20% excess Li by means of the the UHS technique and a conventional furnace. (**E**) Pictures of various ceramics sintered by the UHS technique in ~10 s.

caused by the evaporation of Li and the formation of secondary phases that lead to lower ionic conductivity (*22*). In contrast, the UHS technique enables us to tune the sintering time in units of seconds, which provides excellent control in terms of the Li content and grain growth. As a comparison, we sintered a series of LLZTO precursor formulations featuring 0, 10, and 20% excess Li using either the UHS technique or a conventional furnace. Using inductively coupled plasma mass spectrometry, we observed severe Li loss in the furnace-sintered LLZTO samples (up to 99%) but <4% loss in the UHS samples. This was true even for the sample made without excess Li (Fig. 2D).

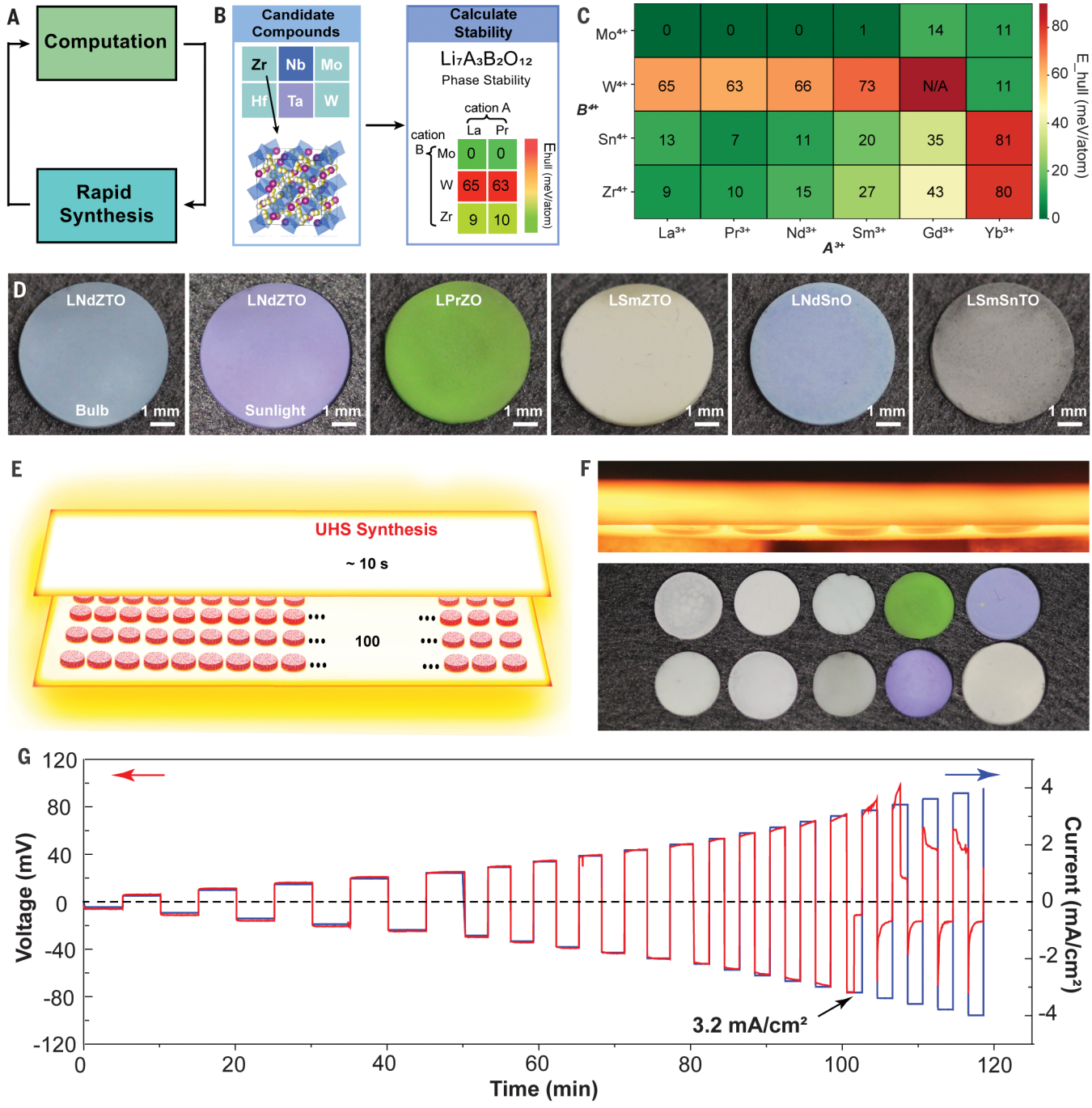


**Fig. 3. Rapid sintering technique for ceramic screening.** (**A**) Accelerated materials discovery enabled by computational prediction and rapid synthesis. (**B**) The computational workflow for predicting new garnet compositions. The phase stabilities of candidate compounds with different cation combinations were evaluated by the energy above hull ($E_{hull}$) in comparison with the lowest-energy phase equilibria. (**C**) The table lists the predicted garnet compositions with different stabilities. (**D**) Pictures of the garnet materials (featuring different colors from the usual white) sintered by means of the UHS technique and predicted by computation. The LNdZTO garnet can change color under different light sources (e.g., a fluorescent light bulb and sunlight) because of the Alexandrite effect (*34*). (**E**) Schematic of a 20 by 5 matrix for cosintering 100 ceramic samples with the UHS technique in just ~10 s. (**F**) Pictures of the UHS setup for cosintering 10 garnet samples. The top image is the side view of the UHS cosintering process. (**G**) The voltage and current profiles of the symmetric cell with a thick Li electrode cycled at different current densities.

The time-of-flight secondary ion mass spectroscopy results confirmed the uniform distributions of all elements in the UHS-sintered LLZTO (fig. S6). Both the densification and Li-evaporation rates increase with temperature as thermally activated processes, but the garnet densification rate likely increases faster than the evaporation rate. This leads to less Li loss with a much shorter sintering time sufficient for densification. The schematic time-temperature-transformation diagram (fig. S7) illustrates the evolution of density and composition of the LLZTO garnet in the UHS process. We identified a pure cubic garnet phase from x-ray diffraction (XRD) patterns of the UHS garnet, whereas the severe Li loss in the conventional furnace–sintered samples leads to a side reaction (fig. S8). Furthermore, the LLZTO samples synthesized with the UHS technique had an ionic conductivity of ~1.0 ± 0.1 mS/cm (fig. S9), which is among the highest reported for garnet-based SSEs (*8*, *18*, *23*).

We can apply our UHS method to synthesize a wide range of high-performance ceramics. As a demonstration, we successfully sintered alumina ($Al_2O_3$, >96% density), $Y_2O_3$-stabilized $ZrO_2$ (YSZ, >95% density, with an ultrafine grain size of 265 ± 85 nm), $Li_{1.3}Al_{0.3}Ti_{1.7}(PO_4)_3$ (LATP, >90% density), and $Li_{0.3}La_{0.567}TiO_3$ (LLTO, >94% density) directly from pressed green pellets of precursor powders and all in under 1 min (Fig. 2E). $Al_2O_3$ and YSZ are two typical structural ceramics with excellent mechanical properties and high sintering temperatures, whereas LATP and LLTO are Li-ion conductors used in solid-state batteries (*3*, *24*). The UHS materials featured pure phases that we identified with XRD, which was indicative of no side reactions (fig. S10). We used scanning electron microscopy (SEM) images to show that the well-sintered grains have low porosity and the fractured cross sections are uniform in microstructure (figs. S11 to S14). The pressureless sintering process and short processing time of the UHS technique also resulted in fewer solid diffusion–related side reactions or sample-carbon heater contamination issues (figs. S15 to S17) than often encountered in SPS (*25*). We hypothesize that the ultrahigh heating rate and short sintering time can kinetically minimize the likelihood of such side reactions. The technique is particularly suitable for high-throughput screening of bulk ceramics compared with different ceramic synthesis techniques.

The ability of the UHS method to rapidly and reliably synthesize a wide range of ceramics enables us to quickly verify new materials predicted by computation and accelerate the screening rate for bulk ceramic materials (Fig. 3A). We used lithium garnet compounds ($Li_7A_3B_2O_{12}$; A = La group, B = Mo, W, Sn, or Zr) as a model system to demonstrate this rapid screening ability that is enabled by computational prediction and the UHS process. We used density functional theory calculations to predict and evaluate the energies of a large number of compounds with other non-Li cation combinations based on garnet structures (Fig. 3B). The phase stabilities of these computer-generated hypothetical $Li_7$-garnet compounds (Fig. 3C) are described by the lower value of the energy above hull ($E_{hull}$), which we determined from the energy difference of the compound in comparison with the stable phase equilibria on the phase diagram (*26*). A material with a small $E_{hull}$ (color-coded green) should feature good phase stability, and a high $E_{hull}$ (color-coded red) suggests an unstable phase. Our compositional screening captured most known stoichiometric $Li_7$-garnets, such as $Li_7La_3Zr_2O_{12}$, $Li_7Nd_3Zr_2O_{12}$, and $Li_7La_3Sn_2O_{12}$ (*18*), which validated the computational method.

We selected the computationally predicted Zr- and Sn-based garnet compositions featuring small $E_{hull}$ values (Fig. 3C) for experimental verification, including $Li_7Pr_3Zr_2O_{12}$ (LPrZO), $Li_7Sm_3Zr_2O_{12}$ (LSmZO), $Li_7Nd_3Zr_2O_{12}$ (LNdZO), $Li_7Nd_3Sn_2O_{12}$ (LNdSnO), and $Li_7Sm_3Sn_2O_{12}$ (LSmSnO). We also synthesized the corresponding 0.5 Ta-doped compositions in the B site [e.g., $Li_{6.5}Sm_3Zr_{1.5}Ta_{0.5}O_{12}$ (LSmZTO)]. New garnet compounds were well synthesized and sintered (figs. S18 to S22) in as little as 10 s, with uniform grain size and microstructure. The final relative densities were in the range of 91 to 96%, with a typical grain size of 2 to 10 μm. We confirmed the garnet structure (cubic phase for B site doped; tetragonal phase for nondoped) using XRD (fig. S23). Our garnet compounds exhibited different optical properties and were not the typical white color, owing to the different La-group elements (Fig. 3D). Our garnets also had ionic conductivities of ~$10^{-4}$ S/cm (e.g., LNdZTO, fig. S24), which are comparable to those of LLZO garnets (*18*, *22*). We also attempted to synthesize some unstable garnet compounds that we predicted by computation, such as $Li_7Gd_3Zr_2O_{12}$. As expected, even though the SEM image shows well sintered grains (fig. S25A), the XRD pattern indicates that the composition did not form the garnet phase (fig. S25B), which verifies our computational predictions.

The fast sintering rate of UHS also enables cosintering of multiple materials simultaneously, which permits even faster screening of materials or devices. In practical ceramic synthesis, sintering can be the most time-consuming process, especially when the optimized sintering parameters have not been developed for new compositions. However, with the UHS sintering technique, 100 ceramic pellets can be rapidly cosintered using a 20 by 5 matrix setup (Fig. 3E), with an area of just ~12 cm by 3 cm (for a pellet size of 5 mm). This setup is practical for materials screening processes. As a demonstration of this scalability, we synthesized 10 garnet compositions (see compositions listed in the supplementary materials) by cosintering directly from the corresponding green bodies (Fig. 3F). In comparison, although SPS is currently considered a high-throughput method to fabricate bulk ceramic specimens, it typically produces just one specimen in ~1 to 2 hours. Moreover, SPS cannot easily be carried out in parallel as it requires multiple expensive SPS instruments.

Ultrafast heating at high temperatures for only seconds can also reduce or eliminate the segregation of detrimental impurities and defects at grain boundaries. This process may have beneficial effects for solid electrolytes and many other structural and functional ceramics. Using LLZTO garnet pellets as a proof of concept, we conducted a symmetric Li stripping-plating study to systematically characterize the electrochemical properties of the UHS garnet SSE. Because of the challenge in diagnosing the short circuit in the symmetric cell configuration (*27*), we applied in situ neutron depth profiling (NDP) (*28*) to confirm that the UHS LLZTO garnet SSE can conduct Li ions at high current densities without short-circuiting (fig. S26, A, B, and C). We show that the Li-LLZTO-Li symmetric cell with a thick (>100 μm) Li metal coating demonstrates a critical current density as high as 3.2 mA/cm$^2$ (Fig. 3G and fig. S26D), which is among the highest reported values for planar garnet-based SSEs (*18*, *29*). We have conducted long-term cycling of the Li-LLZTO-Li symmetric cell (fig. S27), which can cycle for >400 hours at a current density of 0.2 mA/cm$^2$, indicating excellent cycling stability.

Multilayer ceramics have advantages for various applications, including battery electrolytes, but they are challenging to sinter because of interdiffusion at high temperatures. We synthesized a LATP/LLZTO bilayer SSE without detectable side reaction or cross-diffusion using the UHS technique (Fig. 4A). The LLZTO garnet is stable against the Li metal anode, and the LATP features superior oxidation stability compared with the LLZTO (fig. S28) (*30*). Conventional furnace sintering results in severe interdiffusion and side reactions at the interface (fig. S29).

Introducing low–melting point materials into ceramics is a general approach to achieving a dense structure at a lower sintering temperature. We sintered a ceramic composite SSE by adding $Li_3PO_4$ to the LLZTO garnet, in which the $Li_3PO_4$ can melt at ~1200°C and weld with the LLZTO particles to form a dense composite pellet (Fig. 4B) by means of ultrafast liquid-phase sintering, with reduced side reactions and cross-doping compared with the conventional approach (fig. S30).

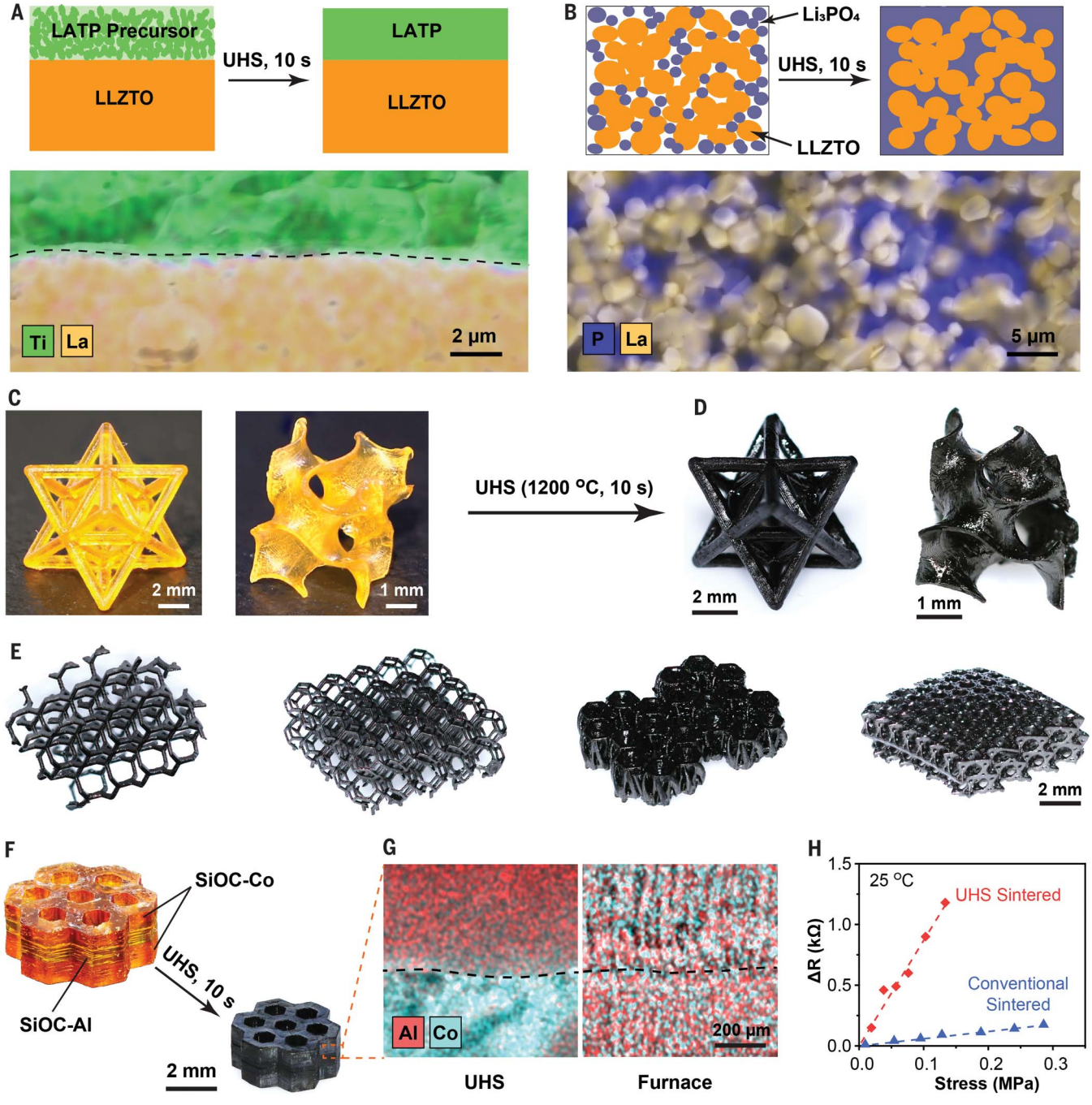


**Fig. 4. Structures enabled by the UHS sintering technique.** (**A** and **B**) Schematics and energy dispersive spectroscopy mapping of the cosintered LATP-LLZTO bilayer SSE (A) and the LLZTO-$Li_3PO_4$ composite SSE (B). (**C**) Photographs of the SiOC polymer precursor printed as a single material. (**D**) Photographs of the SiOC samples sintered by the UHS method, showing the uniform material shrinkage and maintained structures. (**E**) Four UHS-sintered complex structures with different repeating units. (**F**) The multilayer 3D-printed SiOC polymer precursor (doped with Al and Co) and the corresponding UHS-sintered structure. (**G**) Elemental mapping of the Co- and Al-doped boundary of the UHS-sintered and conventional furnace–sintered SiOC samples. (**H**) The piezoresistance versus the stress induced by the magnetic force of the 3D-printed magnetic flux density sensor device sintered by UHS and conventional sintering. ΔR is the change in the piezoresistance.

The UHS technique can also sinter ceramic structures with complex geometries. This is notable because the SPS technique is incompatible with 3D-printed structures. We successfully sintered polymer-derived ceramics (silicon oxycarbide, SiOC) with uniform shrinking and well-maintained structures (Fig. 4, C and D, and movie S2). Additionally, the structures can be stacked to form a more complex 3D lattice design (Fig. 4E). 3D-printed structures and devices with different spatially distributed materials have applications emerging from various combinations of mechanical, thermal, or other properties (*31*–*33*). However, cosintering of these structures is challenging because of cross-diffusion. To explore the capabilities of UHS for such complex designs, we 3D-printed multimaterial honeycomb structures

featuring Al-doped SiOC (for piezoresistivity response) and Co-doped SiOC (for magnetic response, Fig. 4F) to form a magnetic flux sensor (fig. S31). The UHS sintering maintains the perfect registration of the structures with minimal diffusion of dopants caused by the short sintering time (Fig. 4G). Additionally, the 3D-printed magnetic flux sensor device effectively converts magnetic fields into voltage signals (fig. S31). In contrast, the conventional sintering method suffers from substantial diffusion between the different materials (Fig. 4G), which results in poor sensitivity of piezoresistive sensing (Fig. 4H and fig. S31).

The rapid sintering enables the potential for scalable, roll-to-roll sintering of ceramics because the precursor film can quickly pass through the heating strips to achieve continuous UHS. The thin, high-temperature carbon heater in the UHS technique is also highly flexible and can conformally wrap around structures for rapid sintering of unconventional shapes and devices (fig. S32). There are several other potential opportunities. First, UHS can be readily extended to a broad range of nonoxide high-temperature materials, including metals, carbides, borides, nitrides, and silicides, because of its extremely high temperature. Second, UHS may also be used to fabricate functionally graded materials (beyond the simple multilayers demonstrated in this work) with minimum undesirable interdiffusion. Third, the ultrafast, far-from-equilibrium nature of the UHS process may produce materials with nonequilibrium concentrations of point defects, dislocations, and other defects or metastable phases that lead to desirable properties. Finally, this UHS method allows a controllable and tunable temperature profile to enable the control of sintering and microstructural evolution.

## REFERENCES AND NOTES


1. P. B. Vandiver, O. Soffer, B. Klima, J. Svoboda, *Science* **246**, 1002–1008 (1989).
2. E. M. Rabinovich, *J. Mater. Sci.* **20**, 4259–4297 (1985).
3. Z. Zhang *et al*., *Energy Environ. Sci.* **11**, 1945–1976 (2018).
4. A. Manthiram, X. Yu, S. Wang, *Nat. Rev. Mater.* **2**, 16103 (2017).
5. Y. Li, J. T. Han, C. A. Wang, H. Xie, J. B. Goodenough, *J. Mater. Chem.* **22**, 15357–15361 (2012).
6. M. Nyman, T. M. Alam, S. K. McIntyre, G. C. Bleier, D. Ingersoll, *Chem. Mater.* **22**, 5401–5410 (2010).
7. I. Garbayo *et al*., *Adv. Energy Mater.* **8**, 1702265 (2018).
8. X. Huang *et al*., *Energy Storage Mater.* **22**, 207–217 (2019).
9. R. Pfenninger, M. Struzik, I. Garbayo, E. Stilp, J. L. M. Rupp, *Nat. Energy* **4**, 475–483 (2019).
10. R. R. Mishra, A. K. Sharma, *Compos. Part A Appl. Sci. Manuf.* **81**, 78–97 (2016).
11. M. Oghbaei, O. Mirzaee, *J. Alloys Compd.* **494**, 175–189 (2010).
12. O. Guillon *et al*., *Adv. Eng. Mater.* **16**, 830–849 (2014).
13. M. Cologna, B. Rashkova, R. Raj, *J. Am. Ceram. Soc.* **93**, 3556–3559 (2010).
14. D. Angmo, T. T. Larsen-Olsen, M. Jørgensen, R. R. Søndergaard, F. C. Krebs, *Adv. Energy Mater.* **3**, 172–175 (2013).
15. Y. Zhang, J. Nie, J. M. Chan, J. Luo, *Acta Mater.* **125**, 465–475 (2017).
16. M. Yu, S. Grasso, R. Mckinnon, T. Saunders, M. J. Reece, *Adv. Appl. Ceramics* **116**, 24–60 (2017).
17. A. Albrecht, A. Rivadeneyra, A. Abdellah, P. Lugli, J. F. Salmerón, *J. Mater. Chem. C* **4**, 3546–3554 (2016).
18. V. Thangadurai, S. Narayanan, D. Pinzaru, *Chem. Soc. Rev.* **43**, 4714–4727 (2014).
19. W. Ji *et al*., *J. Eur. Ceram. Soc.* **37**, 2547–2551 (2017).
20. A. Sharafi, C. G. Haslam, R. D. Kerns, J. Wolfenstine, J. Sakamoto, *J. Mater. Chem. A* **5**, 21491–21504 (2017).
21. R. P. Rao *et al*., *Chem. Mater.* **27**, 2903–2910 (2015).
22. E. Yi, W. Wang, J. Kieffer, R. M. Laine, *J. Mater. Chem. A* **4**, 12947–12954 (2016).
23. Y. Jin *et al*., *Nat. Energy* **3**, 732–738 (2018).
24. J. C. Bachman *et al*., *Chem. Rev.* **116**, 140–162 (2016).
25. G. Bernard-Granger, N. Benameur, C. Guizard, M. Nygren, *Scr. Mater.* **60**, 164–167 (2009).
26. S. P. Ong, L. Wang, B. Kang, G. Ceder, *Chem. Mater.* **20**, 1798–1807 (2008).
27. P. Albertus, S. Babinec, S. Litzelman, A. Newman, *Nat. Energy* **3**, 16–21 (2018).
28. C. Wang *et al*., *J. Am. Chem. Soc.* **139**, 14257–14264 (2017).
29. N. J. Taylor *et al*., *J. Power Sources* **396**, 314–318 (2018).
30. Y. Zhu, X. He, Y. Mo, *J. Mater. Chem. A* **4**, 3253–3266 (2016).
31. A. Bandyopadhyay, B. Heer, *Mater. Sci. Eng. Rep.* **129**, 1–16 (2018).
32. R. Lakes, *Appl. Phys. Lett.* **90**, 221905 (2007).
33. X. Kuang *et al*., *Sci. Adv.* **5**, eaav5790 (2019).
34. I. P. Roof, M. D. Smith, E. J. Cussen, H. C. zur Loye, *J. Solid State Chem.* **182**, 295–300 (2009).


## ACKNOWLEDGMENTS


We acknowledge the support of the Maryland NanoCenter, its Surface Analysis Center and AIM Laboratory, and the NIST Center for Neutron Research. We also acknowledge M. R. Zachariah and D. J. Kline from the University of California, Riverside, for their contributions to the temperature measurement. **Funding:** This work is not directly funded. J.L. acknowledges support from the Air Force Office of Scientific Research (AFOSR) (FA9550-19-1-0327) and X.Z. acknowledges support from the National Science Foundation (CMMI1727492) and AFOSR (FA9550-18-1-0299).

**Author contributions:** L.H. and C.W. developed the UHS concept and designed the overall experiments. Y.M. and Q.B. conducted the computational predictions and simulation analysis. X.Z. designed the 3D printing experiment. C.W. and W.P. carried out the UHS sintering experiments, electrochemical measurements, and SEM imaging. R.W. helped prepare the samples and conduct the XRD measurements. J.D. created the 3D illustrations. G.P. and J.G. performed XRD characterization. X.W. conducted the temperature profile measurement. H.W. and C.W. performed the NDP measurement. X.Z., H.C., R.H., and Z.X. conducted the material synthesis for 3D printing and characterization. B.Y., C.Z., and Y.P. conducted the measurements of thermal properties and temperature simulations. J.L. contributed to the mechanistic understanding and some sintering experimental designs and analysis. L.H., C.W., A.H.B., Y.M., X.Z., J.L., B.D., and J.-C.Z. collectively wrote and revised the paper. All authors discussed the results and commented on the manuscript. **Competing interests:** The authors declare no competing interests. A provisional patent application, titled "High Temperature Process for Ceramics and other Solid Materials," has been applied for through the University of Maryland (U.S. provisional patent 62/849578). **Data and materials availability:** All data are available in the manuscript or the supplementary materials.

## SUPPLEMENTARY MATERIALS

science.sciencemag.org/content/368/6490/521/suppl/DC1
Materials and Methods
Supplementary Text
Figs. S1 to S32
Tables S1 to S3
References (*35*–*56*)
Movies S1 and S2

8 October 2019; accepted 1 April 2020
10.1126/science.aaz7681

Science

# A general method to synthesize and sinter bulk ceramics in seconds

Chengwei Wang, Weiwei Ping, Qiang Bai, Huachen Cui, Ryan Hensleigh, Ruiliu Wang, Alexandra H. Brozena, Zhenpeng Xu, Jiaqi Dai, Yong Pei, Chaolun Zheng, Glenn Pastel, Jinlong Gao, Xizheng Wang, Howard Wang, Ji-Cheng Zhao, Bao Yang, Xiaoyu (Rayne) Zheng, Jian Luo, Yifei Mo, Bruce Dunn and Liangbing Hu

*Science* **368** (6490), 521-526.
DOI: 10.1126/science.aaz7681

**Speedy ceramic sintering**

Synthesizing ceramics can require heating for long times at high temperatures, making the screening of high-through-put materials challenging. C. Wang *et al.* developed a new ceramic-sintering technique that uses resistive heating of thin carbon strips to ramp up and ramp down temperature quickly. This method allows for the quick synthesis of a wide variety of ceramics while mitigating the loss of volatile elements. Ultrafast sintering is ideal for synthesizing many compositions to screen for ideal properties for a variety of applications, including the development of new solid-state electrolytes.

*Science*, this issue p. 521